Shap. Mem. Superelasticity (2018) 4:428–434
https://doi.org/10.1007/s40830-018-0188-6

Cyclic Properties of Superelasticity in Cu–Al–Mn Single-Crystalline Sheets with Bainite Precipitates

Ryosuke Kainuma[1] · Yohei Yoshinaka[1] · Toshihiro Omori[1]

Published online: 23 August 2018

Abstract Microstructure, Vickers hardness and cyclic superelastic properties at room temperature were examined for Cu-Al-Mn single-crystalline sheets aged at 200 °C for various time periods. The bainite plates started to appear from about 9 ks and the density drastically increased from 18 to 30 ks and the Vickers hardness was strongly affected by the density of the bainite plates. In the sample with a little amount of bainite plates, the superelastic properties were basically similar to those in the bainite-free sample. In the samples with a high density of bainite, however, the transformation critical and hysteresis stresses and the dissipated energy were high and large for the initial stage of cycles, respectively. They drastically and monotonically decreased with increasing cycle number and the residual strain increased from the initial stage, unlike those in the bainite-free sample.

Keywords Cu-based shape memory alloy · Cu-Al-Mn · Bainite · Superelasticity · Functional fatigue

Introduction

Cu-based shape memory alloys (SMAs), such as Cu–Al- and Cu–Zn-based alloys, are attractive for practical applications of the shape memory effect (SME) and superelasticity (SE), because of their low cost [1, 2]. The conventional polycrystalline Cu-based SMAs, however, are known to have neither ductility nor SE strain enough for many applications [3]. The present authors' group reported that the Cu–Al–Mn (CAM) Heusler alloy with a high Mn composition of about 10 at.% and a low Al composition of about 17 at.% shows a high ductility without losing SME, due to an appropriate decrease of the degree of order in $L2_1$-parent phase [4, 5]. In the alloy system, the SM effect and SE are obtained by martensitic transformation from the $L2_1$-parent phase to the 6 M-monoclinic martensite phase. The SE properties have been improved through texture [6] and grain size [7, 8] controls so far, and have already reached the level of the TiNi alloy [5]. Because the CAM alloy can be easily deformed into a complex shape due to its high ductility, it has already been used as a medical device to treat ingrown toenails [9].

In 2013, a novel technique to obtain samples with extremely large grain size over several centimetres was reported for the CAM alloy [10]. In the method, the large grain structure is obtained by only cyclic heat treatment between the β (bcc) single-phase and the β + α (fcc) two-phase region and very recently fabrication of 0.7-m single crystal rods has been achieved [11]. The SE property in the CAM alloy is drastically improved by increase of the relative mean grain size to cross-section area of the sample [7, 8] and an excellent SE property has already been proved in large-scaled samples [11]. The single-crystalline CAM is expected to be used as large parts in the fields of architecture and civil engineering [12].

Electronic supplementary material The online version of this article (https://doi.org/10.1007/s40830-018-0188-6) contains supplementary material, which is available to authorized users.

✉ Toshihiro Omori
omori@material.tohoku.ac.jp

[1] Department of Materials Science, Graduate School of Engineering, Tohoku University, 6-6-02 Aoba-yama, Sendai 980-8579, Japan

For civil engineering application, not only excellent cyclic SE properties, but also high ability of energy absorption, are required to effectively convert vibration mechanical energy to thermal energy during earthquakes. Although the cyclic properties are almost equivalent to those by B19' transformation in the TiNi alloy s [3, 13–15], the area of the stress hysteresis loop in the stress–strain (SS) curve with a flag shape is smaller than that in the TiNi alloy and the energy absorption properties are obviously poorer than those in the TiNi-based alloy [16]. However, Sutou et al. reported that in the CAM alloy, the bainitic transformation appears by low temperature ageing at 200 to 300 °C [17], and that the area of the hysteresis loop in the CAM alloy drastically increases by introduction of the bainite plates with 6 M structure [18]. Also, while SM properties in a temperature cycle of up to 205 °C under a fixed stress were very recently reported by Babacan et al. [19] cyclic SE properties for the as-aged samples with a bainite phase have not been reported.

In the present study, the single-crystalline sheets, which are obtained by abnormal grain growth, were aged at 200 °C for various time periods and the cyclic SE properties at room temperature for the as-aged samples with various amounts of the bainite phase were evaluated by cyclic mechanical test.

Experimental Procedures

An ingot of the Cu-17Al-11.4Mn (at.%) alloy was prepared by induction melting in an argon atmosphere from pure elements, and hot-rolled at 800 °C to a thickness of about 4 mm. The obtained sheet was cold-rolled to 1 mm in thickness with intermediate annealing at 550 °C for 30 min at every 50% reduction. Using a wire electric discharge machine, some samples for the mechanical test were cut from the sheet according to the shape shown in Fig. S1 in the Supporting Information. These samples were subjected to cyclic heat treatment for abnormal grain growth as shown in Fig. S2 to obtain single crystals [10]. The crystallographic orientation in the rolling (and loading) direction in five single-crystalline samples for the mechanical test, named Samples A to E, was determined by an electron backscattered diffraction (EBSD) technique to be near the <110> direction, as shown in the inverse pole figure of Fig. S3a–e. Here, Fig. S3f shows tensile direction dependence of transformation strain reported by Sutou et al. [6]. The loading direction of every sample is almost located in the blue area of Fig. S3f and the transformation strain is expected to be about 7.5 to 9%. The transformation critical stress and stress hysteresis in SE are inversely proportional to the transformation strain [20] which means that their absolute values should be precisely calibrated to make comparisons with one another. In the present study, however, this effect is not taken into account, because of it being negligibly small in comparison to the ageing effect.

Samples A to E for the mechanical test were subsequently annealed at 200 °C for 0.9, 9, 18, 30 and 48 ks, respectively, to obtain the bainite precipitates. While the martensitic transformation temperatures are known to be dependent on the annealing condition, those of the sample annealed for 0.9 ks, with no bainite particle, were determined by differential scanning calorimetry as the forward transformation starting and finishing temperatures, $Ms = -46.3$ °C and $Mf = -71.6$ °C, and the reverse starting and finishing temperatures, $As = -52.4$ °C and $Af = -39.2$ °C. The microstructures of the annealed samples were observed by a secondary electron image obtained via field-emission scanning electron microscopy, where the sample surface was etched by a ferric chloride solution with the composition of $FeCl_3$: 10 g, HCl: 25 ml and H_2O: 100 ml before SEM observation. Vickers hardness test was performed with a weight of 300 gf. The cyclic tensile tests were carried out by a universal testing machine at a strain rate of 8.33×10^{-5} s^{-1} at room temperature, where the maximum strain is fixed to about 5% and performed until the 1000th cycle so as not to fracture the sample.

Results and Discussion

Microstructures and Vickers Hardness

The typical microstructures of the samples aged at 200 °C are shown in Fig. 1. The bainite phase with plate shape starts to appear at 9 ks and almost covers the whole sample at 18 ks. In the sample annealed for 30 ks, the density of the bainite plates further increases and some coarse massive particles start to appear at 48 ks. These coarse particles may be the α-fcc phase transformed from the bainite phase. Figure 2 shows the Vickers hardness of samples annealed at 200 °C for 0.9, 9, 18, 30 and 48 ks. While being almost coincident with that of an as-quenched sample annealed at 0.9 ks, the hardness starts to increase at 9 ks and closes to a steady state of about 48 ks. This behaviour is obviously brought about by the precipitation of the bainite plates. The similar tendency in change of hardness was reported in Cu–16.6Al–9.3Mn–2Ni–0.2B alloy [17], although the onset appears at a slightly shorter ageing time in the previous study. This difference may be explained by the fact that the Cu–16.6Al–9.3Mn–2Ni–0.2B alloy sample is polycrystalline with grain boundaries where the bainite plate easily nucleates [16, 19, 21].

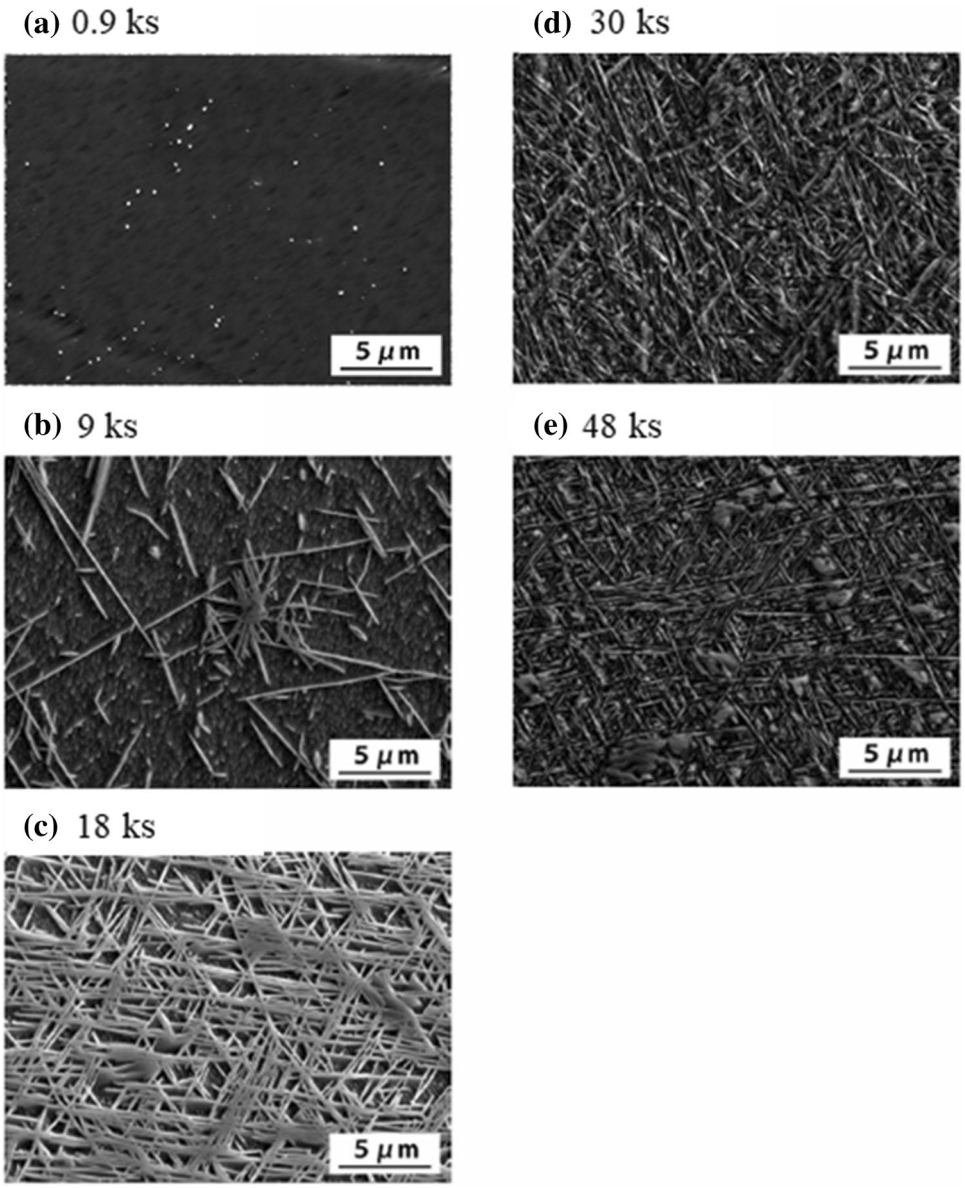

Fig. 1 SEM images taken from samples aged at 200 °C for **a** 0.9, **b** 9, **c** 18, **d** 30 and **e** 48 ks

SE Properties in the 1st cycle

Figure 3 shows the SS curves selected during the cyclic test preformed using Samples A to E, including the data of the first cycle. In the first cycle, we observe that the critical stress, σ_c, of stress-induced transformation (SIT) and the stress hysteresis, σ_{hys}, increase with ageing time, depending on the formation of the bainite plates, as shown in Fig. 4a, where the σ_c and σ_{hys} are defined as shown in Fig. S4. Here, in the SS curve of Sample B, a drastic decrease of stress is detected at around 1.0% strain, as shown in Fig. 3. The origin of this behaviour is unknown, but it may be related to nucleation of the martensite phase. Because the step disappeared after several cycles and the further plateau region had an almost constant value of stress, the lower value after 1.0% strain was used for the σ_c in Sample B. In Sample E, aged for 48 ks, fracture occurs at about 2.5% strain in the first cycle, and no data on SE properties could be obtained.

As shown in Fig. 4a, both σ_c and σ_{hys} start to increase from 9 ks, reaching about 600 and 430 MPa at 30 ks, respectively. These behaviours are very similar to the ageing time tendency in hardness as shown in Fig. 2, which clearly results from the precipitation of the bainite plates. These tendencies are consistent with those reported for the Cu–16.6Al–9.3Mn–2Ni–0.2B alloy wires by Sutou et al. [17]. From the tendency, one can expect the aged samples to show a large dissipated energy, E_{diss}, which is defined by the area of the loop closed in the SS curves, as demonstrated in Fig. S4. The E_{diss} estimated in Samples A to D

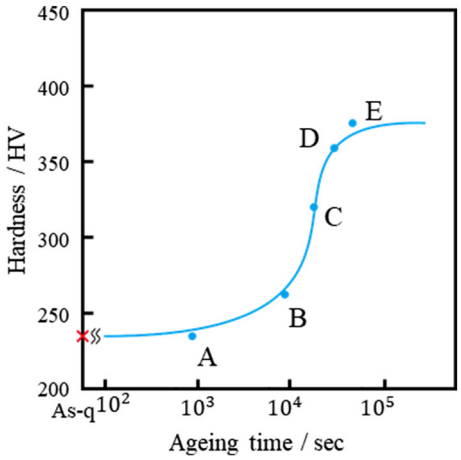

Fig. 2 Vickers hardness of samples aged at 200 °C for 0, 0.9, 9, 18, 30 and 48 ks

are plotted in Fig. 4b. As expected, the ageing time dependence is similar to that of the σ_{hys}. Here, it is worthwhile noting that the maximum E_{diss} for 5% strain reaches a very large value, 16 MJm^{-3}, in Sample D, while being less than 1 MJm^{-3} in Sample A with no bainite plate. This level of E_{diss} is comparable to those in Fe–Ni–Co–Al–Ta–B and Ti–Ni–Nb alloys [16] which are known as SM alloy with the highest level of dissipated energy. Thus, the precipitation of bainite plates drastically increases the E_{diss}. However, one can easily imagine that the sample should receive a large amount of damage by the drastic increase of σ_c. The increase of σ_{hys} also means that the parent/martensite boundary receives a high friction stress in the migration during application of external stress. We found that the residual strain, σ_{hys}, also drastically increases in Samples C and D as well as in the E_{diss}, as shown in Fig. 4b.

Cyclic Properties

All the data on σ_c, σ_{hys}, E_{diss} and ε_{res} that were evaluated from SS curves shown in Fig. 3 are plotted in Fig. 5. In Sample A with no bainite phase, the σ_c basically decreases and shows a dip at about the 50th cycle, while to determine those after 250th cycle is difficult because the plateau is obscure. The σ_{hys} slightly increases to the 150th cycle and then decreases. The behaviour of the E_{diss} is similar to that of the σ_{hys}, but the maximum point occurs at about the 50th cycle. The ε_{res}, however, shows a drastic change unlike the

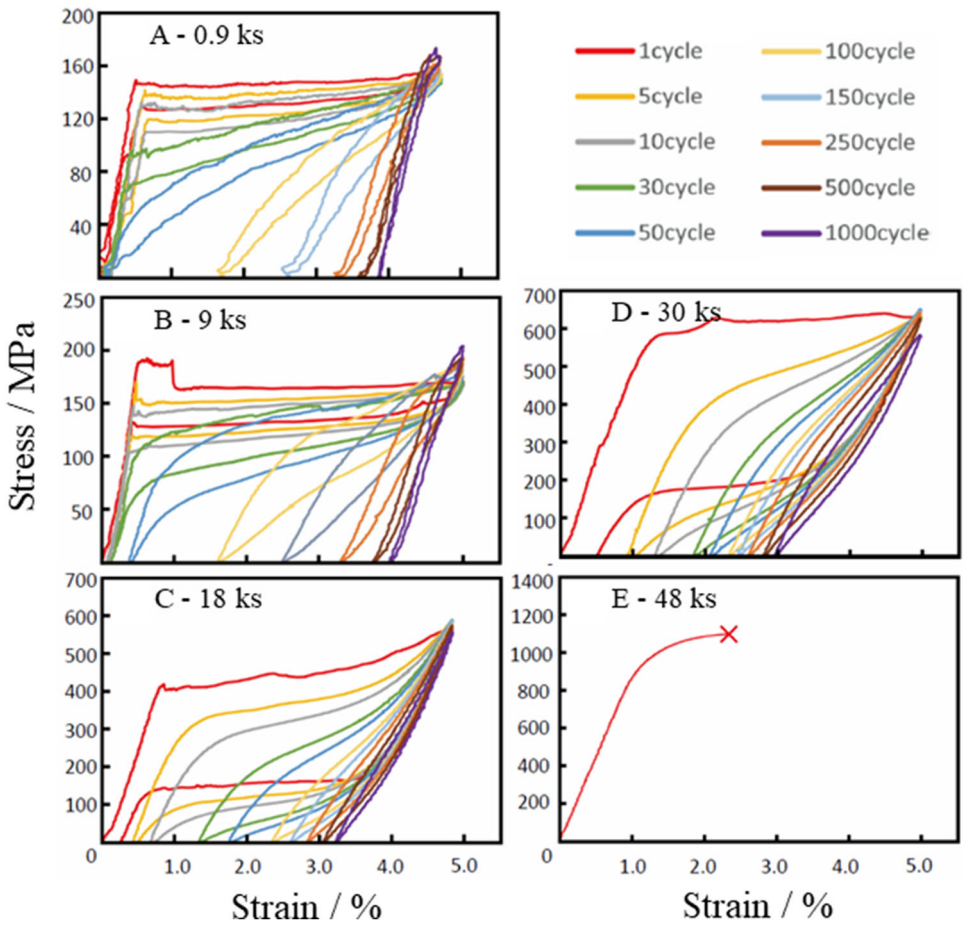

Fig. 3 Stress–strain curves selected from data obtained by a cyclic tensile test of 1000 cycles, where the applied strain is fixed at 5% and Sample E showed fracture in the first cycle

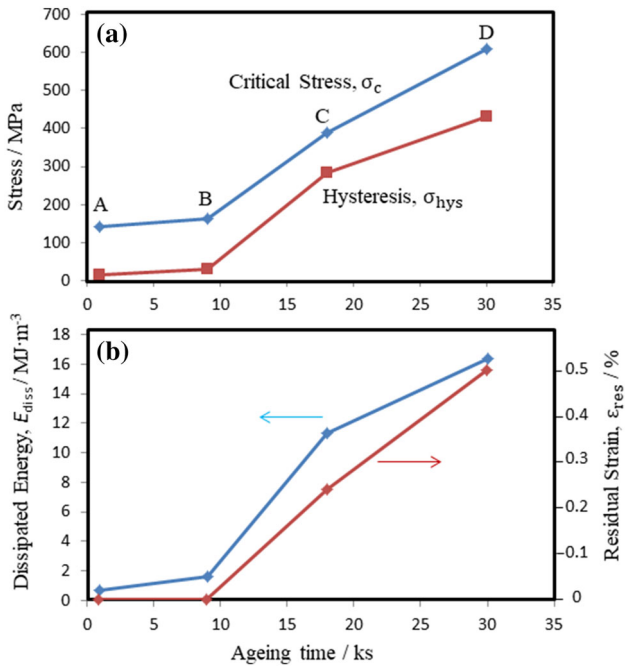

Fig. 4 Ageing time dependence of **a** critical stress and stress hysteresis, and **b** dissipated energy and residual strain in the first cycle extracted from stress–strain curves in Samples A to D of Fig. 3, where the definition of each parameter is presented in Fig. S4

others, i.e. although being negligibly small towards the 50th cycle, the ε_{res} suddenly starts to increase at the 50th cycle. This behaviour is strongly related to the decrease of the σ_c and results from tline 9 he appearance of the retained martensite phase after unloading. In fact, the dip in the σ_c curve is located at the same cycle showing the drastic increase of ε_{res}. However, the increase to the 150th cycle of the σ_{hys} may be brought about by the increase of friction against migration of habit plains by introduction of slip defects. The tendency in these parameters is basically consistent with those reported for polycrystalline alloy by Shrestha et al. [14] and for columnar-grained alloy by Liu et al. [15].

In Sample B, with a low density of the bainite plates, the cyclic dependences on all the parameters are basically similar to those in Sample A, while the σ_c in the final stage drastically increases between 150th and 250th cycle before becoming obscure. The reason for this difference is unclear. Here, it is worthwhile noting that the σ_{hys} and E_{diss} of Sample B are almost twice as large as those of Sample A. This change is obviously due to precipitation of the bainite plates, which makes the friction against the phase boundary motion increase.

The cyclic behaviours in Samples C and D, including a large amount of the bainite plates, are considerably different from those in Samples A and B. The σ_c, σ_{hys} and E_{diss} drastically and monotonically decrease and the ε_{res} increases from the initial stage. It is interesting to note that the ε_{res} curve of Sample C shows an S bend, while that of Sample D is more monotonic. From this tendency in Sample C, the "stage-change" to the active region on the

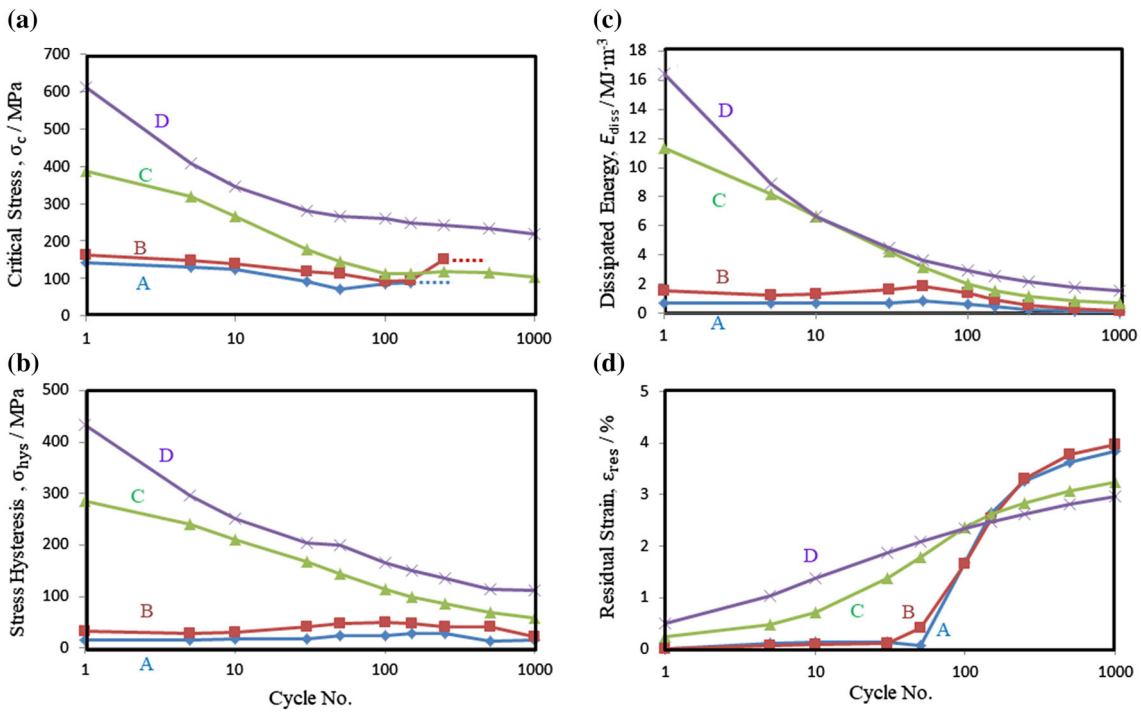

Fig. 5 Cycle dependence of **a** critical stress, **b** stress hysteresis, **c** dissipated energy and **d** residual strain in Samples A to D extracted from stress–strain curves in Fig. 3

appearance of retained martensite, which was detected at about the 50th cycle in Samples A and B, is considered to occur at around the 10th cycle. However, Sample D may already be in the active region even from the initial stage. These results suggest that the samples fully covered by bainite plates receive damage by cyclic stress more easily than the ones with no or a few bainite plates. The deterioration of the SE property in Samples C and D may be caused by higher critical stress as shown in Fig. 5a, because high stress results in much stronger damage to the sample and many dislocations may be induced. In fact, in Sample B with low σ_c, even though some bainite plates are dispersed, as shown in Fig. 1b, all the cyclic behaviours including the ε_{res} are basically coincident with those in Sample A with no bainite. Because slip defects generally stabilize the martensite phase more than the parent phase, the retained martensite, which is the origin of the ε_{res}, starts to appear at the smaller SE cycle number in Samples C and D. The similar cyclic behaviours of σ_c, σ_{hys}, E_{diss} and ε_{res} were also reported in TiNi alloys [22].

Because dissipated energy is directly affected by stress hysteresis, it is important to know the origin of the monotonic decrease in the σ_{hys} shown in Samples C and D of Fig. 5b. Because hysteresis basically comes from friction against migration of habit planes, a decrease of the σ_{hys} means that the friction decreases. However, introduction of dislocations clearly makes the friction increase, because of internal strain around slip defects. However, transformation hysteresis is also known to depend on volume fraction of the martensite phase transformed, i.e. in the case of partial transformation, hysteresis becomes small, depending on the fraction of the martensite transformed [23]. The decrease of σ_{hys} in Samples C and D may be brought about by decrease in the amount of stress-induced martensite, caused by increase of retained martensite.

From these results, we conclude that the dissipation energy is kept relatively high in the initial stage by the introduction of the bainite plates. However, it is not effective to improve fatigue property, and the large hysteresis and dissipated energy in as-aged samples drastically decrease with increasing cycle number. These behaviours are obviously brought about by stabilization of martensite phase due to introduction of dislocations [24, 25]. Because the σ_c in Samples C and D is very high, slip defects are more easily introduced and the SE property may start to deteriorate in the earlier stage than that in the bainite-free sample. To improve the functional fatigue properties, some other hardening techniques, such as solid-solution and/or precipitation hardenings through addition of quaternary elements [26, 27], for preventing the introduction of slip defects are required.

Conclusions

Microstructure, hardness and cyclic superelastic properties at room temperature for Cu–Al–Mn samples aged at 200 °C for 0.9, 9, 18, 30 and 48 ks were examined by SEM observation, Vickers hardness test and cyclic tensile test. The main results are summarized as follows:

1. The bainite plates start to appear from 9 ks and the density drastically increases from 18 to 30 ks. The Vickers hardness is strongly affected by the density of bainite plates in the microstructure and drastically increases from 9 and 30 ks.
2. In the first cycle of the tensile test, the transformation critical stress, σ_c, the stress hysteresis, σ_{hys}, the dissipated energy, $E_{diss,}$ and the residual strain, ε_{res}, start to increase from 9 ks, at which the bainite plates appears, with increasing ageing time. This means that the bainite plates make the E_{diss} increase, but the superelastic properties deteriorate. These tendencies are consistent with those reported in Cu–Al–Mn–Ni–B alloys by Sutou et al. and the level of E_{diss} is comparable to those at the applied strain of 5% in Fe–Ni–Co–Al–Ta–B and Ti–Ni–Nb alloys showing a large E_{diss}.
3. In Sample A, with no bainite, the σ_c basically decreases with a small dip at the 50th cycle, and the σ_{hys} and the E_{diss} gradually increase to the 150th and the 50th cycle, respectively. However, the ε_{res} dramatically increases from about the 50th cycle. Moreover, in Sample B, with a few bainite plates, all the properties are basically similar to those in Sample A without bainite plates, although the σ_{hys} and the E_{diss} are almost twice as large as those in Sample A.
4. In Samples C and D, with a high density of bainite, the σ_c, σ_{hys} and E_{diss} basically decrease and the ε_{res} increases from the initial stage, unlike those in Samples A and B. However, the "stage-change" to the active region on the appearance of retained martensite, which was detected at about the 50th cycle in Samples A and B, appears at around the 10th cycle in Sample C, but from the initial stage in Sample D, and the high performance of E_{diss} is dramatically loss.

Acknowledgements The authors acknowledge support from JSPS KAKENHI Grant Numbers JP15H05766 and JP17H03405.

References

1. Miyazaki S, Otsuka K (1989) Development of shape memory alloys. ISIJ Int 29(5):353–377

2. Tadaki T (1999) Shape memory materialsed. In: Otsuka K, Wayman CM (eds) General applications of SMA's and smart materials. Cambridge University Press, Cambridge, pp 97–116
3. Van Humbeeck J (1999) Shape memory materialsed. In: Otsuka K, Wayman CM (eds) Characteristics of shape memory alloys. Cambridge University Press, Cambridge, pp 149–183
4. Kainuma R, Takahashi S, Ishida K (1996) Thermoelastic martensite and shape memory effect in ductile Cu–Al–Mn alloys. Metall Mater Trans A 27A:2187–2195
5. Sutou Y, Omori T, Kainuma R, Ishida K (2013) Ductile Cu–Al–Mn based shape memory alloys: general properties and applications. Mater Sci Technol 24(8):896–901
6. Sutou Y, Omori T, Kainuma R, Ono N, Ishida K (2002) Enhancement of superelasticity in Cu–Al–Mn–Ni shape-memory alloys by texture control. Metall. Mater. Trans. A 33(9):2817–2824 **(in English)**
7. Sutou Y, Omori T, Yamauchi K, Ono N, Kainuma R, Ishida K (2005) Effect of grain size and texture on pseudoelasticity in Cu–Al–Mn-based shape memory wire. Acta Mater 53(15):4121–4133 **(in English)**
8. Sutou Y, Omori T, Kainuma R, Ishida K (2013) Grain size dependence of pseudoelasticity in polycrystalline Cu–Al–Mn-based shape memory sheets. Acta Mater 61(10):3842–3850
9. Kainuma R (2018) Recent progress in shape memory alloys. Mater Trans 59(3):327–331
10. Omori T, Kusama T, Kawata S, Ohnuma I, Sutou Y, Araki Y, Ishida K, Kainuma R (2013) Abnormal grain growth induced by cyclic heat treatment. Science 341(6153):1500–1502
11. Kusama T, Omori T, Saito T, Kise S, Tanaka T, Araki Y, Kainuma R (2017) Ultra-large single crystals by abnormal grain growth. Nat Commun 8(1):354
12. Araki Y, Endo T, Omori T, Sutou Y, Koetaka Y, Kainuma R, Ishida K (2011) Potential of superelastic Cu–Al–Mn alloy bars for seismic applications. Earthq Eng Struct Dyn 40(1):107–115
13. Kato H, Ozu T, Hashimoto S, Miura S (1999) Cyclic stress–strain response of superelastic Cu–Al–Mn alloy single crystals. Mater Sci Eng A 264(1–2):245–253
14. Shrestha KC, Araki Y, Kusama T, Omori T, Kainuma R (2016) Functional fatigue of polycrystalline Cu–Al–Mn superelastic alloy bars under cyclic tension. J Mater Civ Eng 28(5):04015194 **(in English)**
15. Liu J-L, Huang H-Y, Xie J-X, Xu S, Li F (2017) Superelastic fatigue of columnar-grained Cu–Al–Mn shape memory alloy under cyclic tension at high strain. Scripta Mater 136:106–110
16. Tanaka Y, Himuro Y, Kainuma R, Sutou Y, Omori T, Ishida K (2010) Ferrous polycrystalline shape-memory alloy showing huge superelasticity. Science 327(5972):1488–1490
17. Sutou Y, Koeda N, Omori T, Kainuma R, Ishida K (2009) Effects of ageing on bainitic and thermally induced martensitic transformations in ductile Cu–Al–Mn-based shape memory alloys. Acta Mater 57(19):5748–5758
18. Sutou Y, Koeda N, Omori T, Kainuma R, Ishida K (2009) Effects of aging on stress-induced martensitic transformation in ductile Cu–Al–Mn-based shape memory alloys. Acta Mater 57(19):5759–5770
19. Babacan N, Atli KC, Turkbas OS, Karaman I, Kockar B (2017) The effect of dynamic aging on the cyclic stability of Cu73Al16Mn11 shape memory alloy. Mater Sci Eng A 701:352–358
20. Horikawa H, Ichinose S, Morii K, Miyazaki S, Otsuka K (1988) Orientation dependence of $\beta1 \rightarrow \beta1'$ stress-induced martensitic transformation in a Cu–AI–Ni alloy. Metall Trans A 19(4):915–923
21. Motomura S, Hara T, Omori T, Kainuma R, Nishida M (2016) Morphological and chemical analysis of bainite in Cu-17Al-11Mn (at.%) alloys by using orthogonal FIB-SEM and double-EDS STEM. Microscopy (Oxf) 65(3):243–252
22. Nemat-Nasser S, Guo W-G (2006) Superelastic and cyclic response of NiTi SMA at various strain rates and temperatures. Mech Mater 38(5–6):463–474
23. Dolce M, Cardone D (2001) Mechanical behaviour of shape memory alloys for seismic applications-2. Austenite NiTi wires subjected to tension. Int J Mech Sci 43(11):2657–2677
24. Liu Y, Favier D (2000) Stabilisation of martensite due to shear deformation via variant reorientation in polycrystalline NiTi. Acta Mater 48(13):3489–3499
25. Stalmans R, Van Humbeeck J, Delaey L (1992) Thermomechanical cycling, two way memory and concomitant effects in Cu–Zn–Al alloys. Acta Metall Mater 40(3):501–511
26. Sutou Y, Kainuma R, Ishida K (1999) Effect of alloying elements on the shape memory properties of ductile Cu–Al–Mn alloys. Mater Sci Eng A 273–275:375–379
27. Mallik US, Sampath V (2009) Influence of quaternary alloying additions on transformation temperatures and shape memory properties of Cu–Al–Mn shape memory alloy. J Alloy Compd 469(1):156–163